Earth and Planetary Science Letters 312 (2011) 422–428

Contents lists available at SciVerse ScienceDirect

Earth and Planetary Science Letters

journal homepage: www.elsevier.com/locate/epsl

# Synthesis and equation of state of post-perovskites in the $(Mg,Fe)_3Al_2Si_3O_{12}$ system

Sean R. Shieh [a,*], Susannah M. Dorfman [b], Atsushi Kubo [c,1], Vitali B. Prakapenka [c], Thomas S. Duffy [b]

[a] Department of Earth Sciences, University of Western Ontario, London, ON, Canada N6A 5B7
[b] Department of Geosciences, Princeton University, Princeton, NJ 08544, USA
[c] GeoSoilEnviroCARS, University of Chicago, Chicago, IL 60637, USA

ARTICLE INFO

*Article history:*
Received 18 April 2011
Received in revised form 12 September 2011
Accepted 29 September 2011
Available online xxxx

Editor: L. Stixrude

*Keywords:*
low mantle
D″ layer
post-perovskite
perovskite
iron content
$Al_2O_3$

ABSTRACT

The formation and properties of the post-perovskite ($CaIrO_3$-type) phase were studied in Fe-rich compositions along the pyrope–almandine ($(Mg,Fe)_3Al_2Si_3O_{12}$) join. Natural and synthetic garnet starting materials with almandine fractions from 38 to 90 mol% were studied using synchrotron X-ray diffraction in the laser-heated diamond anvil cell. Single-phase post-perovskite could be successfully synthesized from garnet compositions at pressures above 148 GPa and temperatures higher than 1600 K. In some cases, evidence for a minor amount of $Al_2O_3$ post-perovskite was observed for Alm38 and Alm54 compositions in the perovskite + post-perovskite two-phase region. Pressure–volume data for the post-perovskite phases collected during decompression show that incorporation of Fe leads to a systematic increase of unit cell volume broadly similar to the variation observed in the $(Mg,Fe)SiO_3$ system. The presence of $Al_2O_3$ increases the stability of perovskite relative to post-perovskite, requiring higher pressures (>148 GPa) for synthesis of pure post-perovskites. Our data together with those of Tateno et al. (2005) also suggest that in the Al-rich system the presence of Fe has no strong effect on the pressure required to synthesize the pure post-perovskite phase, but the two-phase perovskite and post-perovskite region may be broad and its width dependent on Fe content. Our results suggest that any regions highly enriched in $Al_2O_3$ may consist of either the perovskite phase or a mixture of perovskite and post-perovskite phases throughout the entire thickness of the D″ region. The observed synthesis pressures (>148 GPa) for a pure post-perovskite phase are beyond that at the Earth's core–mantle boundary (~135 GPa).



## 1. Introduction

The Earth's core–mantle boundary (the D″ layer) is expected to be a complex region of structural heterogeneity and thermal variability (Hirose, 2006; Shim, 2008). The discovery and investigation of the transformation of the $MgSiO_3$ perovskite phase (Pv) to a post-perovskite phase ($CaIrO_3$-type) (pPv) has dramatically altered our understanding of the region (Iitaka et al., 2004; Murakami et al., 2004; Oganov and Ono, 2004; Shim et al., 2004; Wentzcovitch et al., 2006; Wookey et al., 2005). Perovskites and post-perovskites in the deep lower mantle are expected to be chemically complex, and the behavior of post-perovskites across a range of mantle-relevant compositions needs to be investigated in detail to properly interpret seismic data for the deep Earth.

Aluminum is an important chemical constituent of the lower mantle that may be enriched locally in particular regions such as those containing subducted basaltic remnants. In experiments using pyrope ($Mg_3Al_2Si_3O_{12}$) starting material, it was found that a perovskite phase (i.e., $(Mg_{0.75}Al_{0.25})(Al_{0.25}Si_{0.75})O_3$) was stable to 140 GPa, and a single-phase post-perovskite was formed above 170 GPa (Tateno et al., 2005). When compared with $MgSiO_3$, this indicates that the presence of aluminum expands the stability field of perovskite relative to post-perovskite. Other experimental studies of Al-bearing $MgSiO_3$ compositions (with and without Fe) also conclude that the presence of $Al^{3+}$ will broaden and deepen the perovskite to post-perovskite boundary (Andrault et al., 2010; Catalli et al., 2009; Kubo et al., 2007; Nishio-Hamane et al., 2007). Thus, the abundance of aluminum may have important consequences for the D″ region and interpretation of its seismic structure (Andrault et al., 2010; Catalli et al., 2009).

There have been a number of theoretical studies of post-perovskites in the $MgSiO_3$–$Al_2O_3$ system. Using density functional theory calculations, Tsuchiya and Tsuchiya (2008) examined the $MgSiO_3$–$Al_2O_3$ system and found that the addition of moderate amounts of $Al_2O_3$ slightly reduced the Pv–pPv transition pressure and produced a relatively narrow coexistence region for perovskite and post-perovskite. At higher $Al_2O_3$ contents, an $Rh_2O_3$-II-type perovskite phase was stabilized at lower pressures, and an $Al_2O_3$-rich post-perovskite was formed at higher pressures. Other theoretical studies have found a slight increase in the Pv–pPv transition pressure due to addition of $Al^{3+}$ to $MgSiO_3$ (Caracas and Cohen, 2005a,b; Ono and Oganov, 2005; Zhang and Ogonov, 2007). These results stand in

* Corresponding author. Tel.: +1 519 850 2467; fax: +1 519 661 3187.
*E-mail address:* sshieh@uwo.ca (S.R. Shieh).
[1] Present address at Sumitomo Electric Hardmetal Corp. 1-1-1, Koya-kita, Itami, Hyogo 664-0016, Japan.

0012-821X/$ – see front matter © 2011 Elsevier B.V. All rights reserved.
doi:10.1016/j.epsl.2011.09.054

contrast to the experimental studies discussed above which suggest a much stronger effect of aluminum on the phase boundary. However, one earlier theoretical study found that incorporation of $Al^{3+}$ into $MgSiO_3$ pPv would lead to a large increase in transition pressure and coexistence of Pv and pPv over a wide pressure range (Akber-Knutson et al., 2005).

There has also been considerable investigation into the Pv–pPv transition in Fe-containing systems. Features of the deep lower mantle such as large, low-shear velocity provinces, ultra-low velocity zones, subducted slab materials, dense primordial remnants, and core–mantle reaction products (e.g. Garnero and McNamara, 2008; Mao et al., 2005; Nakagawa et al., 2010) could potentially exhibit varying degrees of iron enrichment. In addition to applications to Earth's mantle, the amount of Fe that post-perovskite can accommodate is also relevant to understanding the limits of core sizes in possible super-Earth extrasolar planets (Valencia et al., 2009). Some experimental studies in the $(Mg,Fe)SiO_3$ system suggest that Fe prefers post-perovskite over perovskite thereby reducing the transition pressure and producing a wide Pv–pPv phase loop (Caracas and Cohen, 2005a,b; Mao et al., 2004; Stackhouse et al., 2006) whereas others report a much narrower loop more consistent with a sharp seismic discontinuity (Murakami et al., 2005; Tateno et al., 2007). Variations in Fe oxidation state and also potentially its spin state as well as coupled behavior between Fe and Al add complexity to understanding this chemical component (Catalli et al., 2010a,b; Jackson et al., 2009; Lin et al., 2008; Mao et al., 2010; Sinmyo et al., 2006).

The pyrope–almandine system $(Mg,Fe)_3Al_2Si_3O_{12}$ is $Al_2O_3$-rich (25 mol%) and exhibits complete Mg–Fe solid solution. Natural and synthetic samples with a wide range of Mg# (= Mg/(Mg + Fe)) are available (Hofmeister, 2006; Hofmeister et al., 1998). Here we report an examination of such compositions at deep mantle pressures to provide new insights into the behavior of post-perovskites enriched in both aluminum and iron.

## 2. Experimental method

Three natural garnets with compositions close to the pyrope–almandine join (designated as Alm38, Alm54, and Alm73) (Hofmeister, 2006; Hofmeister et al., 1998) and one synthetic garnet glass (Alm90) were used as starting materials (Table 1). Note that the Alm90 glass contains excess $Al_2O_3$. The natural samples have total grossular and spessartine components of 4–6 mol%. While the amount of ferric iron was not directly measured, the microprobe data suggest the amount of ferric iron in the starting material is small.

The samples were each ground to a fine powder and mixed with ~10 wt.% platinum or gold for use as a pressure calibrant. High pressure and temperature experiments were conducted using laser-heated diamond anvil cells. The sample mixtures were loaded in the 25–35 μm hole of a rhenium gasket, together with NaCl or argon as a pressure medium and sample insulator. Neon gas was loaded for one Alm54 sample with the GSECARS/COMPRES high-pressure gas loading system. In situ high-pressure and high-temperature synchrotron X-ray diffraction experiments were conducted at beamline 13-ID-D of the GSECARS sector, Advanced Photon Source. Double-sided laser heating was used to achieve high temperatures with minimal temperature gradients (Prakapenka et al., 2008; Shieh et al., 2006). Temperatures were measured from both sides of the sample by spectroradiometry. The samples were probed with a monochromatic X-ray beam (wavelength 0.3344 Å) focused to about $5 \times 5\ \mu m^2$ using Kirkpatrick–Baez mirrors. Prior to data collection, the X-ray beam, the center of the heating spot, and the optical paths of the temperature measurement system were carefully aligned using fluorescence generated by the X-rays as they passed through the sample. Two-dimensional X-ray diffraction images were collected at both ambient and high temperatures with a MAR CCD detector. $CeO_2$ powder was used to calibrate the sample-to-detector distance and orientation of the detector. The images were reduced to one-dimensional spectra using the Fit2D program (Hammersley et al., 1996). Diffraction peaks were fit to Voigt lineshapes after background subtraction. The unit cell parameters were obtained by least-squares fit with the UnitCell program. The pressure was determined from the measured *d*-spacings of Pt and Au using their equations of state (Pt) (Fei et al., 2007) and (Au) (Dewaele et al., 2004).

## 3. Results and discussions

Samples were first compressed at room temperature to pressures in excess of 110 GPa. At these conditions, diffraction peaks for all the garnet samples were weak and broad. For each composition, several experiments using different samples (designated as A, B, C, etc.) were carried out. The samples were heated for time periods ranging from 38 to 264 min, and diffraction patterns were collected at both high and room temperatures (Table 2). Note that the pressures listed in the Table 2 represent the maximum pressure achieved during heating in each run and therefore the thermal pressures are considered. In general, due to the high iron contents of the silicate samples, the heating was quite stable and only ~10–40% of the total laser power (100 W) was adequate to heat the sample to 1300–2600 K range. After heating, additional diffraction patterns were recorded both at the heated spot and nearby locations (±6–10 μm). Depending on heating conditions, the CCD images contained relatively smooth or more spotty and heterogeneous rings. Absorption changes accompanying the phase transition sometimes led to runaway heating which resulted in spottier diffraction patterns.

We found that single-phase post-perovskite can be successfully synthesized from all studied garnet compositions at pressures above 148 GPa and temperatures higher than 1600 K (Figs. 1 and 2). Our results demonstrate that the pPv phase can simultaneously accommodate both high aluminum and high iron contents. However, a separate $Al_2O_3$-rich pPv phase was also observed under certain conditions (particularly with heating at 2050 K and below) during some runs for Alm54 and Alm38.

For Alm38A, the sample was compressed to 148 GPa and heated at 1490–1830 K for 60 min. Our results showed that the post-perovskite phase emerged after about 33 min heating, and after temperature quenching the pressure was determined to be ~160 GPa (Fig. 2a). In a separate run, Alm38B was compressed to 160 GPa and heated to 1760–2050 K. The pPv phase was observed during the initial heating

**Table 1**
Chemical compositions of garnet starting materials as determined by electron probe microanalysis.

| | MgO (wt.%) | FeO (wt.%) | $Al_2O_3$ (wt.%) | $SiO_2$ (wt.%) | CaO (wt.%) | MnO (wt.%) | $TiO_2$ (wt.%) | $Cr_2O_3$ (wt.%) | Composition |
|---|---|---|---|---|---|---|---|---|---|
| Alm38 | 15.88 | 18.46 | 23.23 | 39.93 | 1.13 | 0.90 | 0.01 | 0.02 | Alm38Pyr58Grs3Sps2 $(Mg_{0.44}Fe_{0.29}Al_{0.24}Ca_{0.02}Mn_{0.01})(Si_{0.74}Al_{0.26})O_3$ |
| Alm54 | 11.61 | 26.14 | 22.75 | 39.37 | 0.96 | 0.28 | 0.02 | 0.02 | Alm54Pyr43Grs3Sps1 $(Mg_{0.33}Fe_{0.41}Al_{0.24}Ca_{0.02})(Si_{0.74}Al_{0.26})O_3$ |
| Alm73 | 5.28 | 32.84 | 20.47 | 38.86 | 1.65 | 0.61 | 0.02 | – | Alm73Pyr21Grs5Sps1 $(Mg_{0.16}Fe_{0.55}Al_{0.25}Ca_{0.03}Mn_{0.01})(Si_{0.77}Al_{0.23})O_3$ |
| Alm90 | 2.38 | 37.39 | 24.72 | 35.50 | – | – | – | – | Alm90Pyr10 $(Mg_{0.07}Fe_{0.63}Al_{0.3})(Si_{0.71}Al_{0.29})O_3$ |

Alm = almandine, Pyr = pyrope, Grs = grossular, Sps = spessartine. Compositions are given both as endmember proportions in the pyrope–almandine–grossular–spessartine quaternary as well as a recalculation based on the $ABO_3$ stoichiometry of the $CaIrO_3$-type structure. Refs: Alm38 (#36, Table 1, Hofmeister et al., 1998), Alm54 (#40, Table 1, Hofmeister et al., 1998), Alm73 (Al-3, Table 1, Hofmeister, 2006). The Alm90 glass was synthesized in the laboratory of H. O'Neill (Australian National University).

**Table 2**
Summary of experimental observations.

| Sample | Calibrant | Max pressure (GPa) | Temperature (K) | Heating time (min.) | Phases observed |
|---|---|---|---|---|---|
| Alm38A | Pt | 160 | 1490–1830 | 60 | pPv |
| Alm38B | Pt | 154 | 1760–2050 | 30 | pPv, Pv (tr), $Al_2O_3$ pPv (tr) |
| | | 153 | 1630–2030 | 13 | Pv ↑, pPv (w) ↓ |
| Alm38C | Au | 148 | 1600–2560 | 264 | Pv, pPv (w) ↓ |
| Alm54A | Au | 143 | 1520–1670 | 64 | Pv, pPv (tr) |
| Alm54B | Au | 164 | 1290–1780 | 70 | pPv (w) |
| | | 166 | 1660–2110 | 19 | pPv↑ |
| | | 175 | 1670–1880 | 37 | pPv↑ |
| Alm54C | Au | 113 | 1700–2300 | 30 | Pv |
| | | 117 | 1350–1800 | 8 | Pv + pPv |
| Alm54D | Au | 129 | 1900–2200 | 30 | Pv + pPv |
| | | 132 | 1800–2400 | 43 | Pv + pPv |
| | | 150 | 1900–2600 | 50 | pPv + pv(tr) |
| Alm73C | Au | 157 | 2030–2340 | 60 | pPv (w) |
| | | 176 | 2160–2350 | 180 | pPv ↑ |
| Alm73D | Au | 153 | 2280–2400 | 60 | pPv(w) |
| Alm90A | Au | 160 | 1600–2000 | 67 | None |
| | | 180 | 1830–2420 | 116 | pPv ↑ |

w — weak diffraction peaks; tr — trace amount (i.e. very weak diffraction observed, usually only 1 peak)
↑ indicates growth of a phase during heating; ↓ diminishing of a phase during heating.

cycle, especially close to the heating spot. With further heating for ~10 min, peaks assignable to the perovskite phase began emerging, together with new peaks that we assigned to an $Al_2O_3$-rich pPv phase and some other unidentified peaks. The $Al_2O_3$ pPv phase could be identified mainly due to the growth of a shoulder on the 022 peak at 2.3826 Å (Fig. 2b). Other weak $Al_2O_3$ pPv peak positions were also observed in agreement with previously reported values (Ono et al., 2006). Moreover, long heating durations at temperatures of > 1900 K and 153 GPa not only promoted the Pv phase but also enhanced the growth of the $Al_2O_3$ pPv phase. The appearance of $Al_2O_3$ pPv phase indicates some limitation in the capacity to accommodate $Al_2O_3$ in the Pv and pPv phases under these conditions. To evaluate the phase boundary, Alm38B was decompressed to ~132 GPa and heated at 1630–2030 K for 13 min at which time the pPv phase converted to the Pv phase, together with the $Al_2O_3$ pPv phase and other unassigned peaks, and pressure was found to be about 126–127 GPa. For Alm38C, the sample was compressed to 134 GPa and heated at 1600–2500 K. The Pv phase was the dominant phase under these conditions. A weak peak of the pPv 022 was observed at low temperatures but it diminished at higher temperatures, suggesting that the P–T conditions were close to the phase boundary.

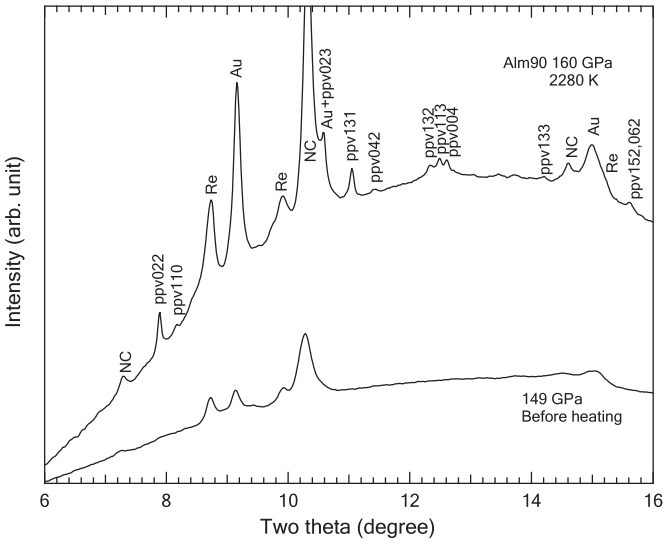


**Fig. 1.** Representative X-ray diffraction patterns of the post-perovskite (pPv) phase synthesized from Alm90 composition. Diffraction patterns are recorded at 300 K from samples quenched at the temperature indicated in the figure. Pressure is measured at 300 K. Post-perovskite phase: pPv, Re: rhenium, Au: gold, and NC: NaCl.

For Alm54A, the sample was compressed to 135 GPa and heated to 1670 K. Only the Pv phase was observed. After further heating for 64 min, the Pv phase remained the dominant phase but a weak pPv 022 appeared at 137–143 GPa and 1460–1600 K. For Alm54B, the sample was compressed to 148 GPa and heated at 1290–1780 K. After about 70 min of stable heating, only weak peaks of the pPv phase were observed. Further heating at 2110 K for 19 more minutes promoted the development of the pPv phase, as evidenced initially by growth of the 131 peak and followed by the development of the 132, 113 and 042 triplet. To synthesize a better quality pPv phase for equation of state study, we then increased pressure to 154 GPa and continuously heated the sample at 1670–1880 K. Our results demonstrated that after 37 min of heating strong pPv peaks were observed and no Pv peaks were present (Fig. 2a). However, scans of the quenched sample showed some unidentified peaks especially in areas where the CCD images show high degrees of preferred orientation. These regions may have been subjected to locally higher temperatures. Note that Alm54B was heated again at 1450–2110 K for another 9 min, the $Al_2O_3$ pPv phase was observed at initial heating but subsequently it disappeared during longer heating. In another run, Alm54C (loaded in a Ne medium) was compressed to 113 GPa and heated to 2300 K for 30 min. During heating, weak peaks of pPv appeared, but disappeared on quench (Fig. 2c). Pressure was then increased to 117 GPa and heating to 1350–1800 K for only 8 min produced a mixture of Pv and pPv that remained after quench (Fig. 2c). This indicates the lower pressure boundary of the Pv–pPv transition for the Alm54 composition is close to ~117 GPa, depending on synthesis temperature. In an additional run (Alm54D), garnet was compressed to 129 GPa and heated for 30 min at 1900–2200 K and a Pv + pPv mixture was confirmed.

Sample Alm73C was loaded in an argon pressure medium and compressed to ~153 GPa and heated at 2030–2340 K for about 60 min. Only weak peaks of the pPv phase were identified at 157 GPa and 2130 K. Next, the sample was compressed to 155 GPa and heated at 2160–2350 K for 120 min. Again, only single pPv phase was observed but the pattern was much stronger (Fig. 2a). Further heating at 2160–2350 K for 60 additional minutes yielded no evidence for minor peaks or the growth of any other phase. This sample was then decompressed gradually and heated at 1750–2470 K for 10–29 min at each decompression step. During this process, the diffraction peaks of the pPv phase remained and no other peaks were observed down to pressures as low as 108 GPa, most likely due to the relatively short heating durations and the slow kinetics of the pPv → Pv transition. The Pv phase emerged below 108 GPa with further heating. In another run, Alm73D (in a NaCl medium) was compressed to ~147 GPa and heated at 2280–2400 K for 60 min. During this run, heating was stable but only weak peaks of the pPv phase were observed despite long heating. The weak pPv phase pattern observed at 153 GPa and 2110 K suggested that the condition may be just above the pPv phase transition boundary.

For Alm90A, sample was compressed to about 149 GPa and heated at 1600–2000 K for 67 min. However, no pPv phase was observed. After further heating for 53 min, a weak pPv phase was observed in quenched patterns with pressure of 159 GPa and no other phase was found in this study. To improve the quality of the diffraction pattern of the pPv phase, we continued to heat the sample for several cycles at temperature of 1830–2420 K with pressures at 172–180 GPa. The lengthy heating resulted in strong growth of the pPv phase and is evident by the quenched patterns shown in Fig. 1. Next, the sample was gradually decompressed without further heating for collecting the pPv volume compression data. A comparison of calculated and measured *d*-spacings for the pPv phase of Alm90 at 160 GPa

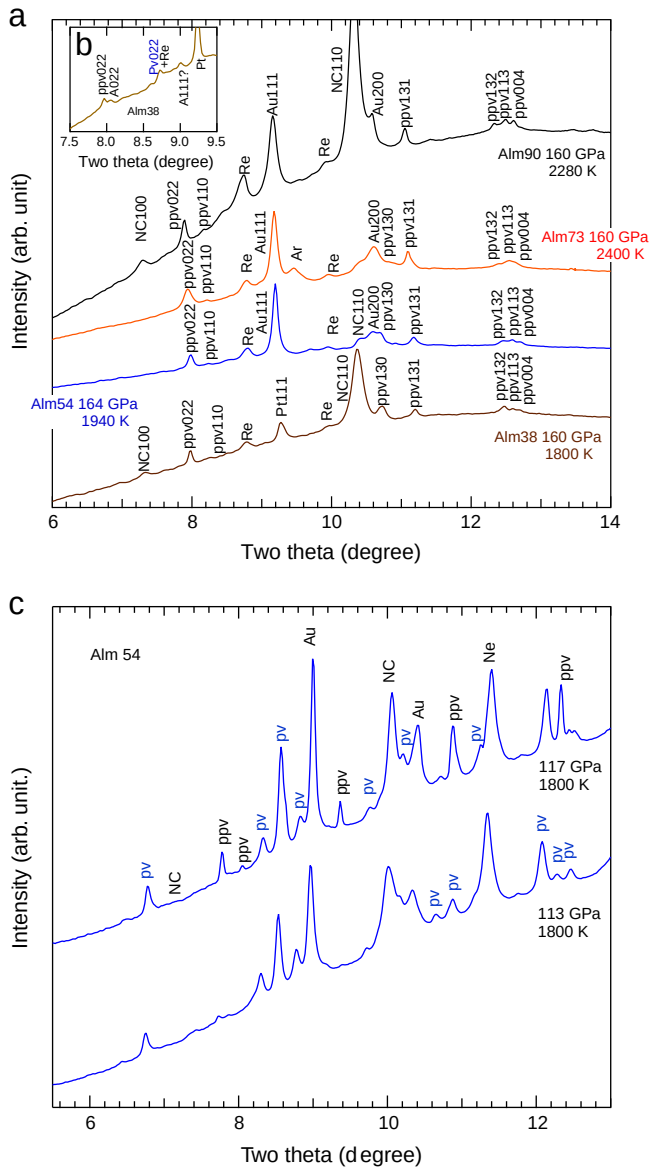


**Fig. 2.** (a) Representative X-ray diffraction patterns of the post-perovskite (pPv) phases synthesized from four compositions along the pyrope–almandine join. (b) (Inset) The $Al_2O_3$ pPv phase was identified from a shoulder on the pPv 022 from a different heating cycle of the Alm38 run shown in (a). (c) Representative X-ray diffraction patterns of the mixture of Pv + pPv phases synthesized from the Alm54 composition. The synthesis temperature conditions for each sample are indicated in the figure. Diffraction patterns are recorded at 300 K from samples quenched at the temperature indicated in the figure. Post-perovskite phase: pPv, $Al_2O_3$ post-perovskite phase: A, perovskite phase: pv, Re: rhenium, Pt: platinum, Au: gold, Ar: argon, NC: NaCl, Ne: neon.

is given in Table 3. Upon decompression, the pPv022 peak became almost undetectable at pressure below 120 GPa followed immediately by the weakening of pPv131 peak. Moreover, the pPv132, 113 and 004 triplets merged into a broad peak and became almost indistinguishable.

Fig. 3 summarizes selected results on the P–T conditions for synthesis of perovskite and post-perovskite phases in the $(Mg,Fe)_3Al_2Si_3O_{12}$ system. The Alm38 compositions showed a Pv + pPv mixed-phase region above 140 GPa and seems to be in agreement with the results of Tateno et al. (2005) for $Mg_3Al_2Si_3O_{12}$. However, our single-phase pPv was synthesized at lower pressure than theirs. During decompression, the pPv phase in Alm38 composition was found to revert back to the Pv phase at about 127 GPa and 1630–2030 K. For Alm54, the mixture phase of Pv + pPv was observed at

**Table 3**
Measured and calculated *d*-spacings of the pPv phase of Alm90 at 160 GPa and room temperature.

| hkl | $d_{obs.}$ | $d_{cal.}$ | $(d_{obs.}-d_{cal})$ |
|---|---|---|---|
| 022 | 2.4306 | 2.4305 | 0.0001 |
| 110 | 2.3484 | 2.3493 | −0.0009 |
| 023 | 1.8150 | 1.8147 | 0.0003 |
| 131 | 1.7370 | 1.7379 | −0.0009 |
| 042 | 1.6820 | 1.6814 | 0.0006 |
| 132 | 1.5583 | 1.5590 | −0.0007 |
| 113 | 1.5379 | 1.5362 | 0.0017 |
| 004 | 1.5219 | 1.5229 | −0.0010 |
| 133 | 1.3529 | 1.3533 | −0.0004 |
| 062 | 1.2300 | 1.2311 | −0.0011 |

$a = 2.457(1)$ Å, $b = 8.075(4)$ Å, and $c = 6.094(2)$ Å.

118 GPa and 1700 K, lower than the Alm38 composition. For Alm73, we successfully obtained single-phase pPv above 153 GPa. During the decompression processes, although heating has been applied on the Alm73 composition at 1750–2470 K for 10–29 min at each decompression step, we still observed the pPv phase down to about 120 GPa. The transformation to the Pv phase may have been kinetically hindered due to relatively short heating interval. For Alm90, as discussed above, the pure pPv phase has been synthesized at 159–180 GPa, in agreement with our other compositions. In general, our results on P–T synthesis conditions for post-perovskite phases are broadly similar to those reported by Tateno et al. (2005) on $Mg_3Al_2Si_3O_{12}$. Pressures above 150 GPa are required for synthesis of single-phase post-perovskite in the almandine–pyrope system at ~1600 K. Thus, the presence of 20–25 wt.% $Al_2O_3$ in these samples increases the stability of perovskite relative to post-perovskite, requiring higher pressures (>150 GPa) for synthesis of pure post-perovskites. In the $(Mg,Fe)SiO_3$ system, the effect of Fe on the Pv–pPv transition pressure has been controversial. Our results together with those of Tateno et al. (2005) suggest that in the Al-rich system, the presence of Fe has little effect on the pressure required to synthesize the pure post-perovskite phase. Nevertheless, the mixture of Pv + pPv found at 118 GPa in the Alm54 composition (Fig. 2c) suggests that the high iron content may lower the pressure of first appearance of pPv coexisting with Pv. Future studies will be needed to examine the phase boundaries in more detail.

These data indicate that the post-perovskite phase can be synthesized from pyrope–almandine starting materials and hence can accommodate at least 20–24 wt.% $Al_2O_3$ and 26–37 wt.% FeO at high P–T conditions. Some studies report significant $Fe^{3+}$ in some aluminous post-perovskites (e.g. Catalli et al., 2009; Nishio-Hamane et al., 2007). Future work is required to assess the site occupancy and valence state of iron in our samples. However, we found no direct evidence for metallic iron that might be expected to accompany formation of large amounts of $Fe^{3+}$ from our starting materials.

Lattice parameters for the post perovskite phase in various compositions are given in Table 4. At least 6 peaks (022, 110, 131, 132, 113 and 004) were used to obtain the unit cell parameters of the pPv phase in this study. Since the data were collected immediately after laser heating, we expect lattice strain effects to be minimal. We observe sharpening of peak widths during heating consistent with reduction of micro-scale differential stresses. Pressure–volume data for the pPv phases collected during decompression are plotted together with other selected data in Fig. 4. Incorporation of Fe leads to a systematic increase of unit cell volume in our samples. The volume increase is due to expansion of all three unit cell axes with Fe incorporation (Table 4). Previous limited work on a pyrope composition showed that the unit cell volume for $(Mg_{0.75}Al_{0.25})(Al_{0.25}Si_{0.75})O_3$ (pyrope) post-perovskite is similar to that of $MgSiO_3$ post-perovskite (Fig. 4) (Guignot et al., 2007; Tateno et al., 2005). Pure $Al_2O_3$ post-perovskite exhibits a slightly lower volume than $MgSiO_3$ post-perovskite (Ono et al., 2006) (Fig. 5). Thus, the unit cell volumes

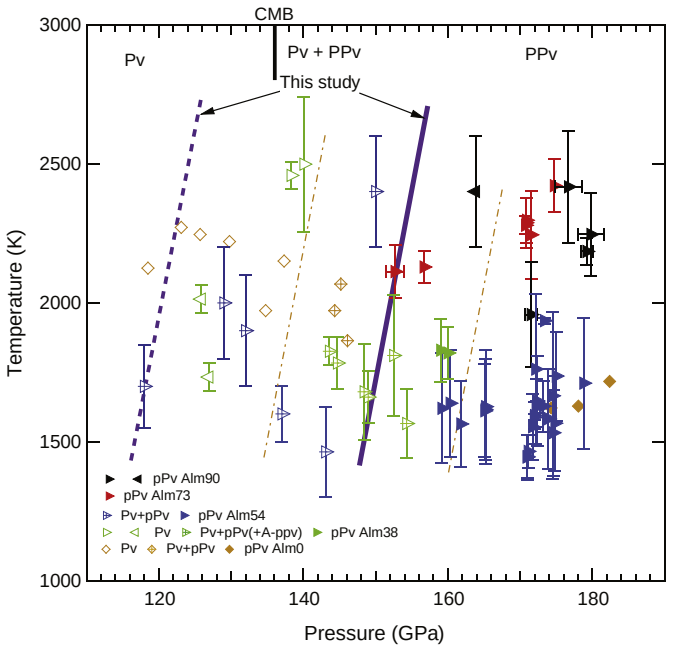


**Fig. 3.** Stability fields of Pv (open symbols), pPv + pPv mixture (open symbols with crosses) and pPv phase (solid symbols) for four different compositions. The dashed line represents the estimated boundary between Pv and Pv + pPv, with the slope from Tsuchiya et al. (2004) and the solid line is the approximate boundary for formation of single-phase pPv. The Alm0 data and dash–dotted lines are from Tateno et al. (2005). Left-pointing triangles: compression data; right-pointing triangles: decompression data. CMB = core–mantle boundary pressure.

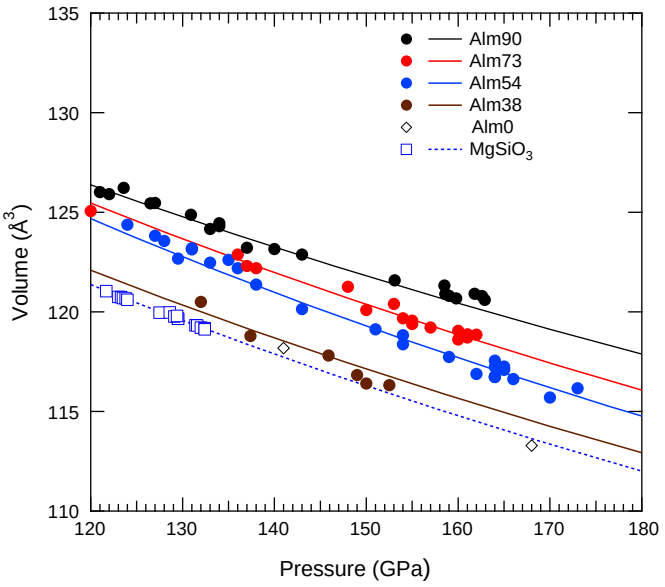


**Fig. 4.** Unit cell volume of the pPv phases synthesized from pyrope–almandine compositions. The symbols are measured data and lines are equation of state fits to the data. The solid circles and lines are from this study. The open diamonds are from Tateno et al. (2005) and the open squares are from Guignot et al. (2007). The error bars are generally smaller than the symbols.

of post-perovskites in the pyrope–almandine system reflect the dominant role of Fe with Al playing a lesser competing role.

Fig. 5 compares data for Alm54 extending below 120 GPa to other studies. The P–V behavior is very similar to earlier reported data on an $(Mg_{0.6}Fe_{0.4})SiO_3$ composition (Mao et al., 2006a) which is expected to have a similar fraction of Fe in the octahedral site (A-site) (see below). In particular, the sharp increase in volume below 100 GPa is observed in both the Al-rich and Al-free samples with high Fe contents. However, this behavior was not observed for a very low-Al Mg#90 sample (Shieh et al., 2006), suggesting this metastable behavior may be connected to high Fe contents. The Alm54 sample was not annealed during decompression below 160 GPa and we observed peak broadening during decompression, and eventually the diffraction peaks were no longer detectable below 41 GPa. For the Alm73 composition, the pPv phase was annealed during decompression and persisted to 108 GPa (without noticeable broadening) until it converted to the Pv phase upon heating. For the Alm90 composition, upon decompression below about 120 GPa, the pPv phase grew increasingly weak and became impossible to detect. Thus, the ability to metastably retain the post-perovskite phase to lower pressures within the perovskite stability field in our compositions is reduced compared to low $Al_2O_3$ compositions and may be affected by iron content (e.g. Mao et al., 2006a,b; Shieh et al., 2006).

The observed variation in volume with Fe content in the $(Mg,Fe)_3Al_2Si_3O_{12}$ system is broadly similar to the variation observed in the $(Mg,Fe)SiO_3$ system (Fig. 5). To illustrate this, Fig. 6 shows the variation in volume for our samples plotted against the Fe# (i.e., Fe/(Fe + Mg + Al)) in the A site for the $ABX_3$ post-perovskite phase at selected pressures. The A-site Fe# for the garnet-composition post-perovskites was determined by assigning all Fe to the A site, and distributing $Al^{3+}$ between the A and B sites for charge balance. The results show that for a given Fe# (A site), higher iron contents exhibit larger volumes in our data, and the pyrope compositions have slightly lower volumes compared to $Al_2O_3$-free samples. On the other hand, pure $MgSiO_3$ pPv volume data exhibit values above the extrapolated trend of our $Al_2O_3$-rich data, but are still lower than those of Fe-rich $Al_2O_3$-free volume data (Mao et al., 2006a,b). This likely reflects the balance between FeO content (which expands the unit cell) and $Al_2O_3$ content (which appears to slightly reduce unit cell volume). However, comparisons with trends from other data sets may be complicated by the use of different pressure calibrants and/or equations of state which can yield significantly different pressures under these conditions.

**Table 4**
Measured unit cell parameters and volume of the post-perovskite phase in various compositions.

| | P (GPa) | *a* (Å) | *b* (Å) | *c* (Å) | V (Å$^3$) | *b*/*a* | *c*/*a* |
|---|---|---|---|---|---|---|---|
| Alm90 | 160 | 2.457(1) | 8.075(4) | 6.094(2) | 120.67(6) | 3.285(3) | 2.480(2) |
| Alm73 | 160 | 2.448(2) | 8.017(12) | 6.066(7) | 119.05(7) | 3.275(8) | 2.478(5) |
| Alm54 | 159 | 2.448(8) | 7.933(6) | 6.061(2) | 117.74(6) | 3.240(13) | 2.476(9) |
| Alm38 | 150 | 2.432(1) | 7.914(9) | 6.048(4) | 116.40(10) | 3.254(5) | 2.487(3) |
| Alm0[a] | 168 | 2.415(0) | 7.817(2) | 6.001(2) | 113.29(7) | 3.237(1) | 2.485(1) |
| (Mg,Fe)(Al,Si)pPv[b] | 172 | 2.430(1) | 7.896(5) | 6.045(2) | 115.99(16) | 3.249(3) | 2.488(2) |
| $MgSiO_3$[c] | 132 | 2.450 | 7.9933 | 6.0837 | 119.12 | 3.263 | 2.484 |

[a] $Mg_{0.75}Al_{0.5}Si_{0.75}O_3$ Tateno et al., 2005.
[b] $Mg_{0.85}$ $Fe_{0.15}Al_{0.15}Si_{0.85}O_3$ Nishio-Hamane et al., 2007.
[c] Guignot et al., 2007.

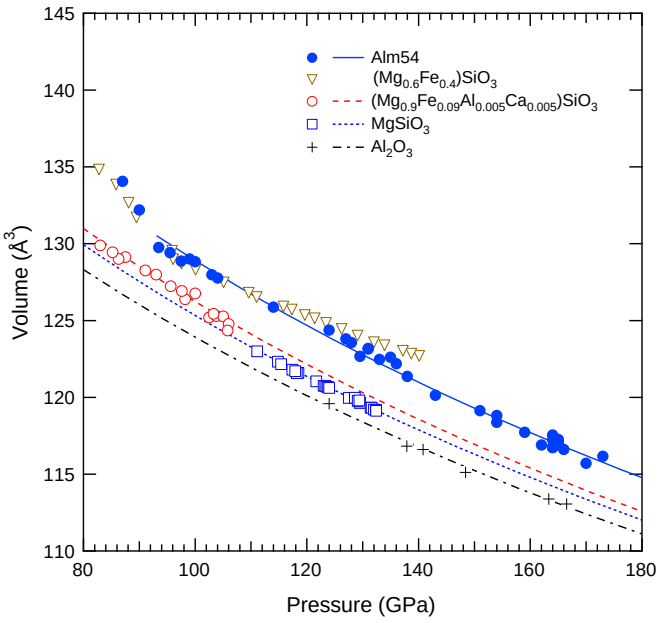


**Fig. 5.** Measured unit cell volumes of the pPv phases extended to metastable conditions. The solid circles and line are from this study. The open triangles are from Mao et al., 2006a; open circles from Shieh et al. (2006); open squares from Guignot et al. (2007) and crosses from Ono et al. (2006). The error bars are smaller than the symbol size.

In summary, X-ray diffraction experiments on laser-heated samples at pressures up to ~180 GPa demonstrate that a $CaIrO_3$-type post-perovskite phase can be synthesized for compositions along the pyrope–almandine join up to at least 90 mol% almandine at above 150 GPa and 1600 K. The presence of 20–25 wt.% $Al_2O_3$ in these samples increases the stability of perovskite relative to post-perovskite, requiring higher pressures (>150 GPa) for synthesis of pure post-perovskites. Between ~120 and 150 GPa, mixtures of Pv and pPv are usually observed but the diffraction patterns are generally weak even with prolonged heating, suggesting a broad mixed phase region with sluggish kinetics as suggested by Tateno et al. (2005) for pyrope. Overall, the transformation kinetics for the $Al_2O_3$-rich samples appear to be more sluggish than for orthopyroxene starting compositions, and thus further work at establishing phase boundaries is required. Finally, we note that any regions highly enriched in $Al_2O_3$ may consist of perovskite or a mixture of Pv and pPv phases throughout the entire thickness of D″ as suggested in other recent studies (Andrault et al., 2010; Catalli et al., 2009). The synthesis pressures (>150 GPa) for a pure pPv phase are greater than that encountered at Earth's core mantle boundary (~135 GPa).

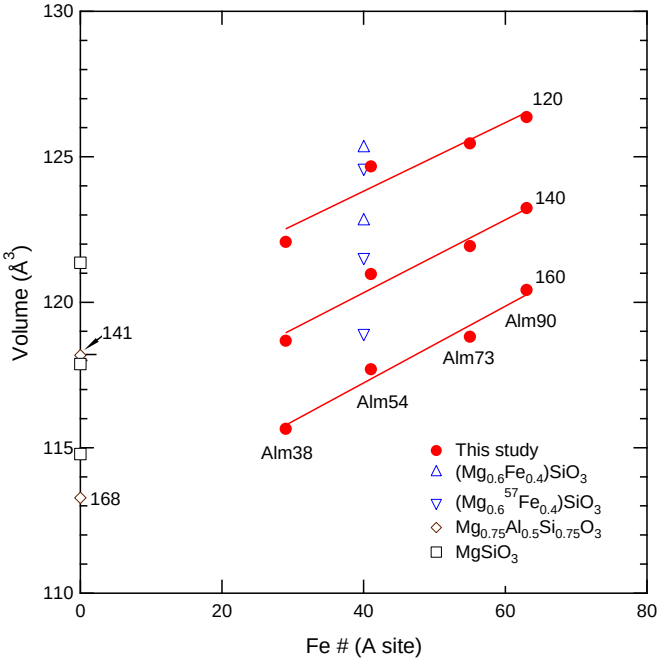


**Fig. 6.** Unit cell volumes as a function of A-site Fe # for $ABO_3$ post-perovskites at 120–160 GPa. A-site Fe# is calculated assuming all Fe is in the A (8-fold) site and $Al^{3+}$ is distributed evenly between the octahedral and 8-fold sites providing charge balance according to $2Al^{3+} \rightarrow (Mg^{2+}, Fe^{2+}) + Si^{4+}$. Values at 120, 140 and 160 GPa were obtained by using the fitted Birch–Murnaghan equation of state from our experimental data. Solid lines are linear fits at each pressure. Open triangles are from Mao et al. (2006a,b) who used two separate synthetic samples, one enriched in $^{57}Fe$ (2006b). The reported volumes for these two samples are ~1% different. Open diamonds (labeled with 141 and 168 in GPa) are from Tateno et al. (2005). Open squares are from Guignot et al. (2007) and correspond to 120, 140, and 160 GPa from fits to their data. Pressures (in GPa) are indicated next to each line.

## Acknowledgments

The natural garnet samples were kindly provided by Anne Hofmeister (Washington University) and the glass sample was synthesized in the laboratory of Hugh O'Neill (Australian National University). This work was supported by NSERC and NSF (EAR-0838017). GeoSoilEnviroCARS is supported by the National Science Foundation — Earth Sciences (EAR-0622171) and Department of Energy — Geosciences (DE-FG02-94ER14466). Use of the Advanced Photon Source was supported by the U. S. Department of Energy, Office of Science, Office of Basic Energy Sciences, under Contract No. DE-AC02-06CH11357.

## References

Akber-Knutson, S., Steinle-Neumann, G., Asimow, P.D., 2005. Effect of Al on the sharpness of the $MgSiO_3$ perovskite to post-perovskite phase transition. Geophys. Res. Lett. 32, L14303. doi:10.1029/2005GL023192.

Andrault, D., Munoz, M., Bolfan-Casanova, N., Guignot, N., Perrillat, J., Aquilanti, G., Pascarelli, S., 2010. Experimental evidence for perovskite and post-perovskite coexistence throughout the whole D″ region. Earth Planet. Sci. Lett. 293, 90–96.

Caracas, R., Cohen, R.E., 2005a. Prediction of a new phase transition in $Al_2O_3$ at high pressures. Geophys. Res. Lett. 32, L06303.

Caracas, R., Cohen, R.E., 2005b. Effect of chemistry on the stability and elasticity of the perovskite and post-perovskite phases in the $MgSiO_3$–$FeSiO_3$–$Al_2O_3$ system and implications for the lower mantle. Geophys. Res. Lett. 32, L16310.

Catalli, K., Shim, S.-H., Prakapenka, V.B., 2009. Thickness and Clapeyron slope of the post-perovskite boundary. Nature 462, 782–785.

Catalli, K., Shim, S.-H., Prakapenka, V.B., Zhao, J., Sturhahn, W., Chow, P., Xiao, Y., Liu, H., Cynn, H., Evans, W.J., 2010a. Spin state of ferric iron in $MgSiO_3$ perovskite and its effect on elastic properties. Earth Planet. Sci. Lett. 289, 68–75.

Catalli, K., Shim, S.-H., Prakapenka, V.B., Zhao, J., 2010b. X-ray diffraction and Mossbauer spectroscopy of $Fe^{3+}$-bearing Mg-silicate post-perovskite at 128–138 GPa. Am. Mineral. 95, 418–421.

Dewaele, A., Loubeyre, P., Mezouar, M., 2004. Equations of state of six metals above 94 GPa. Phys. Rev. B 70, 094112.

Fei, Y., Ricolleau, A., Frank, M., Mibe, K., Shen, G., Prakapenka, V., 2007. Toward an internally consistent pressure scale. Proc. Natl. Acad. Sci. U. S. A. 104, 9182–9186.

Garnero, E.J., McNamara, A.K., 2008. Structure and dynamics of Earth's lower mantle. Science 320, 626–628.

Guignot, N., Andrault, D., Morard, G., Bolfan-Casanova, N., Mezouar, M., 2007. Thermoelastic properties of post-perovskite phase $MgSiO_3$ determined experimentally at core–mantle boundary P–T conditions. Earth Planet. Sci. Lett. 256, 162–168.

Hammersley, A.P., Svensson, S.O., Hanfland, M., Fitch, A.N., Häusermann, D., 1996. Two-dimensional detector software: from real detector to idealised image or two-theta scan. High Pressure Res. 14, 235–248.

Hirose, K., 2006. Postperovskite phase transition and its geophysical implications. Rev. Geophys. 44, RG3001. doi:10.1029/2005RG000186.

Hofmeister, A., 2006. Thermal diffusivity of garnet at high temperature. Phys. Chem. Miner. 33, 45–62.

Hofmeister, A.M., Schaal, R.B., Campbell, K.R., Berry, S.L., Fagan, T.J., 1998. Prevalence and origin of birefringence in 48 garnets from the pyrope–almandine–grossularite–spessartine quaternary. Am. Mineral. 83, 1293–1301.

Iitaka, T., Hirose, K., Kawamura, K., Murakami, M., 2004. The elasticity of the $MgSiO_3$ post-perovskite phase in the Earth's lowermost mantle. Nature 430, 442.

Jackson, J.M., Sturhahn, W., Tschauner, O., Lerche, M., Fei, Y., 2009. Behavior of iron in (Mg, Fe)$SiO_3$ post-perovskite assemblages at Mbar pressures. Geophys. Res. Lett. 36, L10301.

Kubo, A., Duffy, T.S., Shen, G., Prakapenka, V., 2007. Stability and Equation of State of Post-perovskite Phase in the System $MgSiO_3$–$Al_2O_3$ to 2 Mbar, EOS Trans. AGU, Fall Meeting Suppl., MR23D-07.

Lin, J.F., Watson, H., Vanko, G., Alp, E.E., Prakapenka, V.B., Dera, P., Struzhkin, V.V., Kubo, A., Zhao, J., McCammon, C., Evens, W.J., 2008. Intermediate-spin ferrous iron in lowermost mantle post-perovskite and perovskite. Nat. Geosci. 10, 688–691.

Mao, W.L., Mao, H.-K., Strurhahn, W., Zhao, J., Prakapenka, V.B., Shu, J., Hemley, R.J., 2006b. The effect of pressure on the structure and volume of ferromagnesian post-perovskite. Geophys. Res. Lett. 33, L12S02. doi:10.1029/2006GL025770.

Mao, W.L., Mao, H.-K., Prakapenka, V.B., Meng, Y., Shu, J., Fei, Y., Hemley, R.J., 2006a. Iron-rich post-perovskite and the origin of ultralow-velocity zones. Sciences 312, 564–565.

Mao, W.L., Meng, Y., Shen, G., Prakapenka, V.B., Campbell, A.J., Heinz, D.L., Shu, J., Caracas, R., Cohen, R.E., Fei, Y., Hemley, R.J., Mao, H.-K., 2005. Iron-rich silicates in the Earth's D″ layer. Proc. Natl. Acad. Sci. U. S. A. 102, 9751–9753.

Mao, W.L., Shen, G., Prakapenka, V.B., Meng, Y., Campbell, A.J., Heinz, D.L., Shu, J., Hemley, R.J., Mao, H.-K., 2004. Ferromagnesian postperovskite silicates in the D″ layer of the Earth. Proc. Natl. Acad. Sci. U. S. A. 101, 15867–15869.

Mao, Z., Lin, J.F., Jacobs, C., Watson, H.C., Xiao, Y., Chow, P., Alp, E.E., Prakapenka, V.B., 2010. Electronic spin and valence states of Fe in $CaIrO_3$-type silicate post-perovskite in the Earth's lowermost mantle. Geophys. Res. Lett. 37, L22304. doi:10.1029/2010GL054021.

Murakami, M., Hirose, K., Sata, N., Ohishi, Y., 2005. Post-perovskite phase transition and mineral chemistry in the pyrolitic lowermost mantle. Geophys. Res. Lett. 32, L03304. doi:10.1029/2004GL021956.

Murakami, M., Hirose, K., Kawamura, K., Sata, N., Ohishi, Y., 2004. Post-perovskite phase transition in $MgSiO_3$. Science 304, 855–858.

Nakagawa, T., Tackley, P.J., Deschamps, F., Connolly, J.A.D., 2010. The influence of MORB and harzburgite composition on thermo-chemical mantle convection in a 3-D spherical shell with self consistently calculated mineral physics. Earth Planet. Sci. Lett. 296, 403–412.

Nishio-Hamane, D., Fujino, K., Seto, Y., Nagai, T., 2007. Effect of the incorporation of $FeAlO_3$ into $MgSiO_3$ perovskite on the post-perovskite transition. Geophys. Res. Lett. 34, L12307. doi:10.1029/2007GL029991.

Oganov, A.R., Ono, S., 2004. Theoretical and experimental evidence for a post-perovskite phase of $MgSiO_3$ in Earth's D″ layer. Nature 430, 445–448.

Ono, S., Oganov, A.R., 2005. In situ observations of phase transition between perovskite and $CaIrO_3$-type phase in $MgSiO_3$ and pyrolitic mantle composition. Earth Planet. Sci. Lett. 236, 914–932.

Ono, S., Oganov, A.R., Koyama, T., Shimizu, H., 2006. Stability and compressibility of the high-pressure phases of $Al_2O_3$ up to 200 GPa: implications for the electrical conductivity of the base of the lower mantle. Earth Planet. Sci. Lett. 246 (3), 326–335.

Prakapenka, V.B., Kubo, A., Kuznetsov, A., Laskin, A., Shkurikhin, O., Dera, P., Rivers, M.L., Sutton, S.R., 2008. Advanced flat top laser heating system for high pressure research at GSECARS: application to the melting behavior of germanium. High Pressure Res. 28, 225–235.

Shieh, S.R., Duffy, T.S., Kubo, A., Shen, G., Prakapenka, V.B., Sata, N., Hirose, K., Ohishi, Y., 2006. Equation of state of the postperovskite phase synthesized from a natural $(Mg, Fe)SiO_3$ orthopyroxene. Proc. Natl. Acad. Sci. U. S. A. 103, 3039–3043.

Shim, S.-H., 2008. The postperovskite transition. Annu. Rev. Earth Planet. Sci. 36, 569–599.

Shim, S.-H., Duffy, T.S., Jeanloz, R., Shen, G., 2004. Stability and structure of $MgSiO_3$ perovskite to the core–mantle boundary. Geophys. Res. Lett. 31, L10603. doi:10.1029/2004GL019639.

Sinmyo, R., Hirose, K., O'Neill, H.S., Okunishi, E., 2006. Ferric iron in Al-bearing post-perovskite. Geophys. Res. Lett. 33, L12S13. doi:10.1029/2006GL025858.

Stackhouse, S., Brodholt, J.P., Price, G.D., 2006. Elastic anisotropy of $FeSiO_3$ end-members of the perovskite and post-perovskite phases. Geophys. Res. Lett. 33, L01304. doi:10.1029/2005GL023887.

Tateno, S., Hirose, K., Sata, N., Ohishi, Y., 2005. Phase relations in $Mg_3Al_2Si_3O_{12}$ to 180 GPa: effect of Al on post-perovskite phase transition. Geophys. Res. Lett. 32, L15306. doi:10.1029/2005GL023309.

Tateno, S., Hirose, K., Sata, N., Ohishi, Y., 2007. Solubility of FeO in (Mg, Fe)SiO3 perovskite and post-perovskite phase transition. Phys. Earth Planet. Inter. 160, 319–325. doi:10.1016/j.pepi.2006.11.010.

Tsuchiya, J., Tsuchiya, T., 2008. Postperovskite phase equilibria in the $MgSiO_3$–$Al_2O_3$ system. Proc. Natl. Acad. Sci. U. S. A. 105, 19160–19164.

Tsuchiya, T., Tsuchiya, J., Umemoto, K., Wentzcovitch, R.M., 2004. Phase transition in $MgSiO_3$ perovskite in the Earth's lower mantle. Earth Planet. Sci. Lett. 224, 241–248.

Valencia, D., O'Connell, R.J., Sasselov, D.D., 2009. The role of high-pressure experiments on determining super-Earth properties. Astrophys. Space Sci. 322, 135–139.

Wentzcovitch, R.M., Tsuchiya, T., Tsuchiya, J., 2006. $MgSiO_3$ postperovskite at D″ conditions. Proc. Natl. Acad. Sci. U. S. A. 103, 543–546.

Wookey, J., Stackhouse, S., Kendall, J.M., Brodholt, J., Price, G.D., 2005. Efficacy of the post-perovskite phase as an explanation for lowermost-mantle seismic properties. Nature 438, 1004–1007.

Zhang, F., Ogonov, A.R., 2007. Mechanisms of $Al^{3+}$ incorporation in $MgSiO_3$ postperovskite at high pressures. Earth Planet. Sci. Lett. 248, 69–76.